IRAQI JOURNAL OF APPLIED PHYSICS
Vol. 22, No. 3, July-September 2026, pp. 413-421

Influence of Precursor Concentration on Structural and Morphological Properties of Eco-Friendly Synthesized Magnesium Oxide Nanoparticles

**Reger A. Ramadhan*
Sabah M. Ahmed**

Department of Physics,
College of Science,
University of Duhok,
Duhok, Kurdistan Region, IRAQ
*Corresponding author Email:
regrabdullrahman2017@gmail.com

This study presents an eco-friendly green synthesis of magnesium oxide nanoparticles (MgO NPs) using *Prunus persica* leaf extract, investigating the critical role of precursor concentration (0.15–0.4 M) in tuning their structural, morphological, and optical properties. XRD confirmed the formation of a pure cubic MgO phase, with crystallite size increasing from 10.83 nm to 36.14 nm as precursor concentration rose. SEM revealed that 0.3 M yielded well-defined, spherical nanoparticles (~87 nm) The 0.3 M precursor concentration is optimal because it balances nucleation and growth, allowing phytochemicals to effectively cap Mg^{2+} ions—producing uniform, well-crystallized, defect-free MgO nanoparticles with the highest stability and bandgap (5.40 eV), while other concentrations resulted in agglomeration. EDX verified near-stoichiometric Mg:O ratios at 0.3 M, and FTIR confirmed biomolecule-assisted synthesis. UV-Visible analysis showed a strong absorption peak near 214 nm, with the optimal bandgap of 5.40 eV achieved at 0.3 M. These findings highlight 0.3 M as the ideal precursor concentration for synthesizing high-quality, stable MgO NPs via this sustainable route - offering promising potential for catalytic, biomedical, and environmental applications.

Keywords: Magnesium oxide; Nanoparticles; Green synthesis; Plant extract; Precursor concentration
Received: 3 September 2025; Revised: 8 December; Accepted: 15 December; Published: 1 July 2026

1. Introduction

Nanoscience and nanotechnology are expanding research disciplines that involve devices, systems, and structures with various properties. Scientists are focusing on these areas and their various applications. [1,2]. Nanoscale materials are often employed in sectors such as catalysis, electronics, coatings, petrochemicals, and composite production. They also have essential uses in biology and medicine, including as sensors, medical imaging instruments, targeted medication delivery, antimicrobial agents, and dye removal [3,4]. The biosynthesis method is safer and further environmentally friendly; it could be a more reliable substitute for chemical and physical methods [5]. However, physical techniques demand high pressure and high temperatures, which are relatively expensive [6]. On the contrary, Chemical techniques have a negative effect since they employ chemical material as reducing agent, which causes several problems for the ecosystem and the users [7]. Plant extraction is a comparatively green and eco-friendly process for producing several types of nanoparticles. Various plant components, such as roots, stems, leaves, and fruits, as well as microorganisms including bacteria, fungi, yeast, algae, and even proteins, are frequently utilized as natural reducing agents in nanomaterial production [8]. The leaf extract contains biomolecules that play a crucial role in reducing metal salts into metal oxide nanoparticles [1,5]

. Magnesium oxide nanoparticles (MgO NPs) are considered harmless for humans and animals. There are many techniques to producing MgO NPs, including hydrothermal [9], laser's deposition [10], sol-gel [11,12], aerosol (Helble, 1998), spray Pyrolysis [13], chemical vapour deposition [14], sonochemistry [15], and green synthesis [16]. It is worth mentioning, the green synthesis has been a significant technique in the production of metal oxide nanoparticles because it costs less with fewer chemical toxins and improved environmental sustainability. Relying on the advantages, there has been a notable interest in researching the green synthesis of magnesium oxide nanoparticles [17,18]. Magnesium oxide (MgO), which is an alkaline earth metal oxide, crystallizes in a cubic structure and exhibits a wide direct band gap of 7.8 eV [19,20]. Furthermore, the melting point of MgO is 3,125 K, and its boiling point is 3,873 K, resulting in excellent chemical stability and electrical resistivity. The antibacterial, biomedical, and photocatalytic properties of MgO NPs are among their significant applications [16,18,21]. Green synthesis using plant extracts follows a well-established three-step mechanism. During the reduction process, the bioactive molecules from the plant extract reduce the metal ions to their atomic state. In the nucleation phase, these newly formed atoms come together, creating small but stable clusters that serve as growth centres. Finally, the process concludes with phytochemicals acting as natural capping agents, which direct how the particles grow and prevent them from aggregating uncontrollably [22].

Based on the current literature, the green synthesize of MgO nanoparticles using *Prunus persica* leaf extract has not yet been reported. In the current work, MgO NPs were successfully synthesized through this novel green route, and the impact of varying precursor concentrations on their structural, morphological, and optical properties was thoroughly investigated. This environmentally benign biosynthetic route offers a sustainable alternative to conventional chemical methods while enabling tunable nanoparticle characteristics through precursor optimization.

2. Materials and Methods

In October 2023, fresh *Prunus persica* leaves were collected from Grbish Village (coordinates: 36.80951, 43.96248), located in the east of Akre in the Duhok governorate of the Kurdistan Region of Iraq. The starting materials for this research were magnesium nitrate hexahydrate (Mg $(NO_3)_2 \cdot 6H_2O$, 256.42 g/mol, >99.0% purity) and sodium hydroxide pellets (NaOH, 40 g/mol). The materials were used in their original commercial form, without any contamination or alteration, thereby maintaining their specialized status. Distilled water is employed throughout the experiment.

Fresh leaves from the *Prunus Persica* plant were washed many times with tap and distilled water to clear away any dirt and pollution. Fresh *Prunus persica* leaves (60 g) were washed thoroughly with tap water followed by distilled water to remove surface contaminants, then air-dried at room temperature for 1 h. The dried leaves were cut into small fragments and mixed with 480 mL of distilled water (1:8 w/v ratio). The mixture was heated at 70 °C for 25 min under continuous magnetic stirring (500 rpm). After cooling to ambient temperature, the extract was filtered through Whitman No. 1 filter paper (pore size: 11 µm) to remove solid debris. The filtrate was stored at 4 °C in a dark bottle for further use (Fig. 1a). In the end, Refrigerated and set aside for further testing processes was the filtered extract.

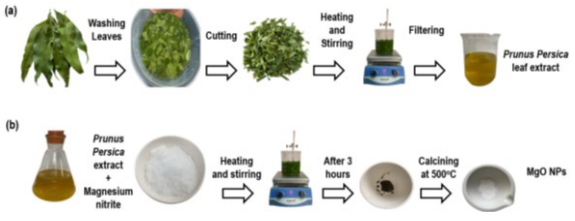

Fig. (1) Preparation steps of (a) plant extract, (b) synthesis of MgO NPs

The extraction parameters (1:8 w/v, 70°C, 25 min) were optimized based on prior protocols for polyphenol-rich leaf extracts [23], ensuring maximal solubilization of bioactive compounds while minimizing thermal degradation.

According to results obtained by Wani Arif et al, phytochemical screening indicates that the leaves of *Prunus persica* are rich in flavonoids, saponins, carbohydrates, alkaloids, and tannins. Those natural compounds work as both reducing agents and stabilizers during nanoparticle formation. They significantly control the size and stability of the nanoparticles [23].

The extraction parameters (1:8 w/v, 70°C, 25 min) were adapted from established protocols for polyphenol-rich leaf extracts [23], balancing efficient biomolecule solubilization with thermal degradation avoidance. Preliminary tests confirmed maximal UV-Visible absorbance under these conditions.

The characteristic of biosynthesised MgO NPs is influenced by the concentrations of magnesium precursor salts. In this investigation, different molar concentrations of magnesium nitrate hexahydrate (MNH) (0.15, 0.2, 0.25, 0.3, and 0.4 M) were used with *Prunus persica* aqueous extract to synthesize MgO NPs, as follows: First, 50 mL of *Prunus persica* aqueous extract (constant volume) was added to 50 mL of each MNH aqueous solution in a 250 mL beaker with magnetic stirring. A 1 M aqueous solution of NaOH was prepared and added dropwise (at a rate of 0.5 mL/min) to the mixture under continuous stirring (500 rpm), while continuously monitoring the pH using a calibrated digital pH meter (Hanna HI2211). The pH was adjusted to 9.0±0.1 to facilitate the hydrolysis of Mg^{2+} to $Mg(OH)_2$ and enhance the deprotonation of phenolic groups in the leaf extract, thereby improving their reducing and capping efficiency [23]. The mixture was blended and heated at 75°C for three hours. Following that, the leftover mixture was calcined in a furnace at 500°C for two hours to produce pure magnesium oxide nanoparticles. Finally, the MgO NPs product was kept in a tube to be characterized. Figure 1b explains in detail how MgO NPs are synthesized. The sample IDs for MgO nanoparticle samples with varying precursor concentrations are listed in table (1).

Table (1) Synthesis conditions for MgO nanoparticles prepared at different precursor concentrations

Sample	Precursor Concentration (mol/L)	Volume of *Prunus persica* Extract (mL)	Total Reaction Volume (mL)
A	0.15	50	100
B	0.20	50	100
C	0.25	50	100
D	0.30	50	100
E	0.40	50	100

The reaction pH was adjusted to 9 because: (i) Mg^{2+} hydrolyzes to $Mg(OH)_2$ above pH ~9–10, facilitating precursor conversion; and (ii) many phytochemical capping agents (e.g., phenolics) are deprotonated at alkaline pH, enhancing their reducing and stabilizing capacity [24].

The crystal structure of the synthesized MgO NPs was investigated through X-ray diffraction analysis (XRD). The surface characteristics were examined

using scanning electron microscopy (SEM), while energy-dispersive X-ray spectroscopy (EDX) verified the elemental composition of the samples. To understand the chemical bonding, the FTIR spectroscopy measurements were applied on both the *Prunus persica* leaf extracts and the resulting MgO nanoparticles, scanning from 400 to 4000 cm^{-1} in transmittance mode. Optical properties were investigated using a double-beam UV-Visible spectrophotometer (Model 6850, JANEWAY, Cole-Parmer Ltd., Staffordshire, UK) operating within the 190-1100 nm wavelength range.

All syntheses were performed in triplicate to ensure reproducibility. Crystallite sizes (XRD), particle sizes (SEM), band gaps (UV-Visible), and EDX atomic ratios were averaged over three independent samples. Results are reported as mean ± standard deviation (SD). For SEM, particle sizes were measured using ImageJ software across ≥100 particles per sample.

3. Results and Discussion

To the best of our knowledge, this is the first report on the green synthesis of MgO nanoparticles using *Prunus persica* leaf extract with a systematic investigation of precursor concentration effects on structural, morphological, and optical properties. While *Prunus persica* has been used for the synthesis of Ag and Fe_3O_4 nanoparticles [24,25], its application for MgO remains unexplored. Figure (2), UV-Visible spectrum, revealed characteristic absorption peaks at 248 nm and 316 nm, confirming the presence of phytochemicals, particularly absorption at 248 nm and 316 nm is characteristic of π→π transitions in conjugated systems of flavonoids and polyphenols, consistent with prior reports on *Prunus* species, which function as both reducing and capping agents due to their antioxidant properties, facilitating nanoparticle formation and stabilization [26,27].

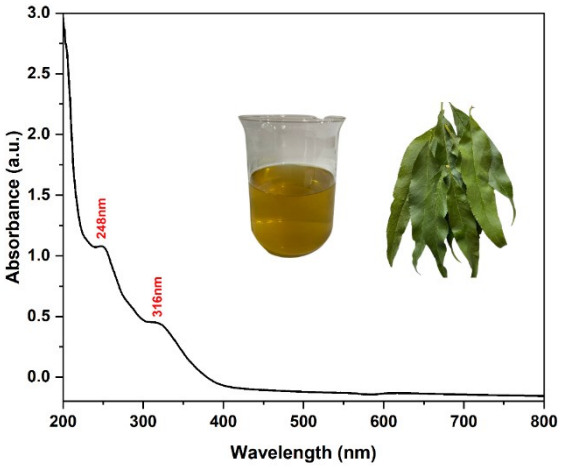

Fig. (2) UV-Visible spectrum of *Prunus persica* leaf extract

FTIR spectroscopy was applied to examine the *Prunus persica* leaf extract and identify which functional groups were present in its biomolecules. Figure (3) displays the FTIR spectrum of the extract, which reveals several distinct peaks in the range of 400 to 4000 cm^{-1}. The observed peaks were located at 628.18, 1079.23, 1121.47, 1271.68, 1644.32, 2065.38, 3399.65, 3526.40, 3565.80 and 3625.21 cm^{-1}. FTIR analysis further identified key functional groups involved in the synthesis, the peak at 628 cm^{-1} is assigned to Mg-O lattice vibrations in the rock-salt structure of MgO, consistent with literature reports for nanocrystalline MgO [28]. Other peaks include 3412 cm^{-1} (O–H stretching), 2922 and 2851 cm^{-1} (C–H stretching), 1641 and 1616 cm^{-1} (C=C stretching in aromatic rings), and 1383 cm^{-1} (carboxylate stretching), confirming the presence of residual phytochemicals that act as capping agents, The persistence of organic functional groups (C–H, C=O, O–H) after calcination at 500 °C suggests strong chemisorption of biomolecules onto MgO surfaces, forming stable complexes that resist thermal decomposition - a phenomenon previously reported in green-synthesized metal oxides [26]. Amine and hydroxyl groups (1079.23 cm^{-1}), C–N stretching in amines (1121.47–1271.68 cm^{-1}), C=O stretching in acid anhydrides (1644.32 cm^{-1}), N–H stretching in amino acids (2065.38 cm^{-1}), and broad O–H stretching in alcohols (3399.65–3625.21 cm^{-1}), all of which corroborate the active role of plant-derived biomolecules in reducing magnesium nitrate to MgO nanoparticles [29,30].

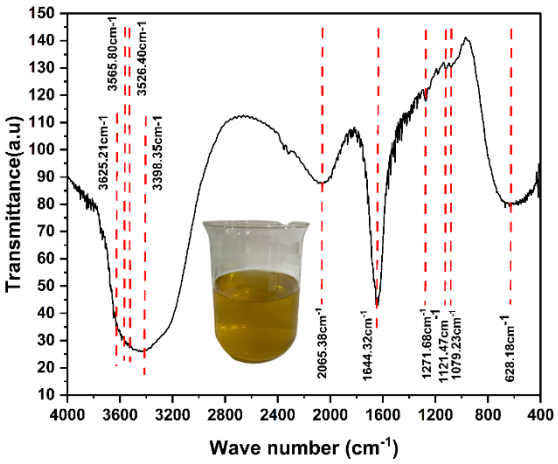

Fig. (3) FTIR spectrum of *Prunus persica* leaf extract

The XRD patterns of MgO NPs at various precursor concentrations are shown in Fig. (4). The peaks at 2θ = 36.85°, 42.81°, 62.17°, 74.52°, and 78.43° were indexed to the (111), (200), (220), (311), and (222) planes, respectively. demonstrating the creation of a well-defined cubic crystalline structure in nano-MgO [31,32].

XRD patterns were recorded using a Bruker D8 Advance diffractometer with Cu Kα radiation (λ = 1.5406 Å), operating at 40 kV and 40 mA, with a step size of 0.02° and scan rate of 2°/min in the 2θ range of

20°-80°. Crystallite sizes were calculated using the Scherrer's equation:

$$D = \frac{K\lambda}{\beta\cos\theta} \quad (1)$$

where K=0.9 (shape factor for cubic crystals), λ is the X-ray wavelength, β is the full-width at half maximum (FWHM) in radians, and θ is the Bragg's angle

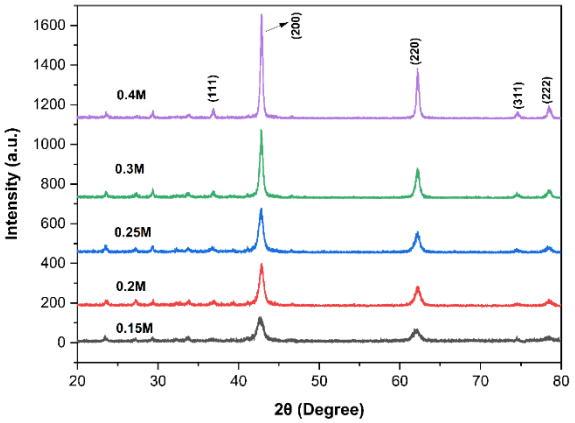

Fig. (4) XRD patterns of MgO NPs for different concentrations

The FWHM values (after instrumental broadening correction using a Si standard) and calculated crystallite sizes are listed in table (2). The (200) peak was used for all calculations due to its highest intensity and minimal overlap. The average crystallite sizes for samples A–E were determined as 10.8±0.9, 18.1±1.2, 19.7±1.1, 27.1±1.5, and 36.1±2.0 nm, respectively. No detectable peaks corresponding to $Mg(OH)_2$ (e.g., at ~38° 2θ) or $MgCO_3$ were observed, confirming phase-pure cubic MgO (ICDD PDF-4+ 2023, Card No. 01-087-0651) [33].

Figure (5) shows that crystallite size increases proportionally with precursor concentration due to enhanced Mg^{2+} availability, while minimal impurities were attributed to residual $Mg(OH)_2$ or surface chemical bonds [31,32,34,35]. The crystallite size derived from XRD (27.10 nm for sample D) is significantly smaller than the particle size observed via SEM (~87 nm), indicating that individual SEM particles are polycrystalline aggregates composed of multiple coherently diffracting domains. This is common in green-synthesized metal oxides, where biomolecular capping limits primary crystallite growth but does not prevent secondary agglomeration during drying or calcination.

A calcination temperature of 500°C was selected based on previous studies of MgO NP synthesis [34], which show complete decomposition of $Mg(OH)_2/MgCO_3$ precursors and crystallization of MgO above 450°C. Although TGA of the precursor was not performed here, XRD confirmed phase-pure MgO with no residual hydroxide peaks (e.g., no broad feature at ~38° 2θ).

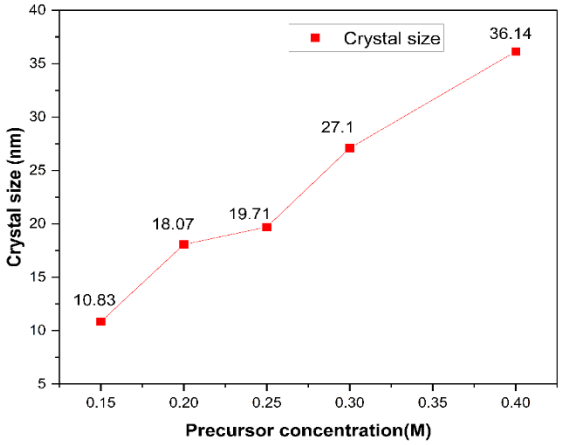

Fig. (5) Crystallite size versus precursor concentration

SEM was employed to analyze the surface morphology of the biosynthesized MgO NPs, as depicted in Fig. (6). The study was carried out on materials synthesised with different precursor concentrations and *Prunus persica* leaf extract as a capping and stabilizing agent. Only sample (d) had a distinct and detectable particle size distribution (Fig. 6e) having an average particle size of around 86.94 nm and a mainly spherical shape. The remaining samples (a, b, c, and e) exhibited substantial agglomeration, making it impossible to identify a definite particle size distribution.

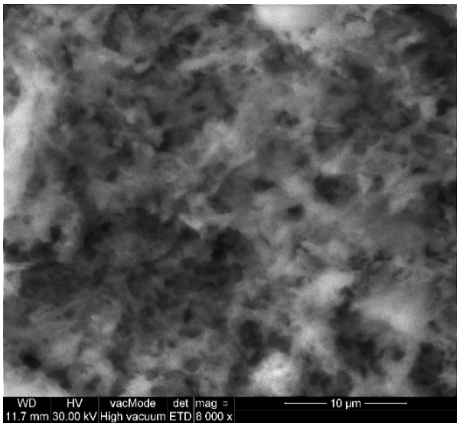

(a)

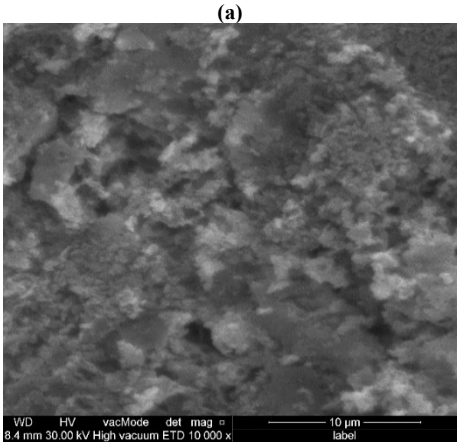

(b)

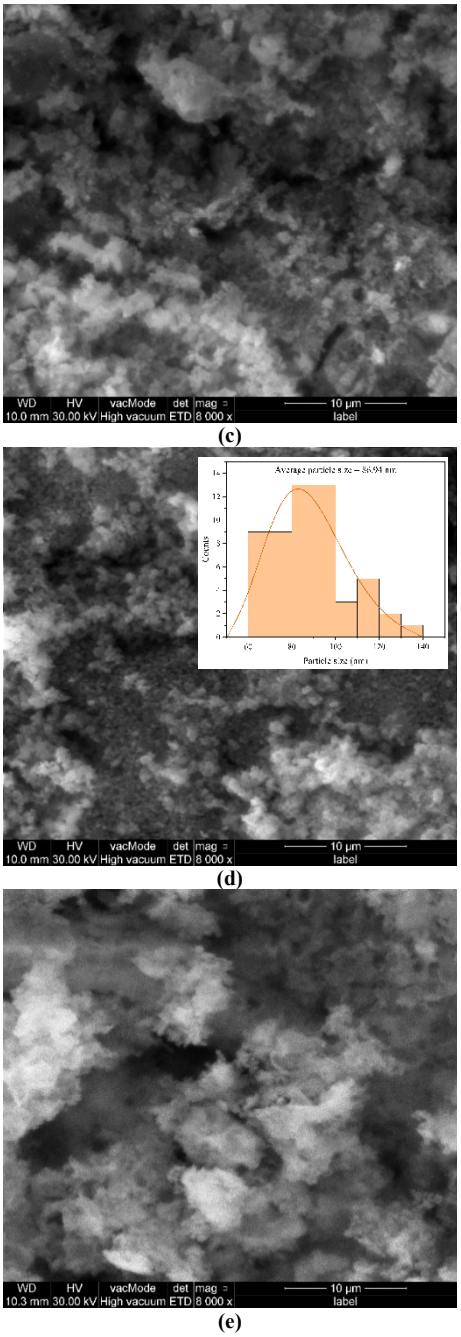

Fig. (6) The SEM images of the green synthesized MgO NPs

The increase in crystallite size with precursor concentration suggests a shift from nucleation-dominated to growth-dominated regimes. At low concentrations (e.g., 0.15 M), high supersaturation favors rapid nucleation, yielding numerous small crystallites. As precursor concentration increases, the reduced nucleation rate (due to lower relative supersaturation) allows existing nuclei to grow larger via Ostwald ripening where smaller, less stable crystallites dissolve and re-deposit onto larger ones. The 0.3 M condition may represent an optimal balance: sufficient Mg^{2+} for growth, yet enough capping biomolecules (flavonoids, polyphenols) from the leaf extract to stabilize nuclei and limit uncontrolled aggregation. In contrast, at 0.4 M, excess Mg^{2+} likely overwhelms the capping capacity of the extract, leading to rapid, anisotropic growth and agglomeration (as seen in SEM).

We propose that the spherical, non-agglomerated morphology at 0.3 M arises from an optimal Mg^{2+}:biomolecule ratio. Phytochemicals such as flavonoids (evidenced by UV-Visible spectroscopy at 248/316 nm and FTIR carbonyl/O–H stretches) adsorb onto nascent MgO nuclei, providing electrostatic and steric stabilization. Below 0.3 M, insufficient precursor limits particle yield and growth. Above 0.3 M, the fixed extract volume cannot fully cap the increased surface area of growing particles, resulting in agglomeration - consistent with DLVO theory and prior green synthesis studies [12,32].

The apparent particle size in SEM reflects agglomerates of primary crystallites, as confirmed by the XRD-Scherrer analysis. Thus, the spherical morphology at 0.3 M refers to well-defined agglomerates with uniform shape and minimal fusion, suggesting effective surface passivation by phytochemicals at this concentration.

EDX was used to determine the elemental composition of the biosynthesized MgO NPS, as illustrated in Fig. (7). The MgO NPs were synthesized using peach leaf extract at different precursor concentrations. When the samples were analyzed with EDX spectroscopy, it was found that magnesium and oxygen were seen as the main elements in all samples, including small amounts of potassium. The expected peaks for magnesium and oxygen appeared in the 0.5–1.5 keV energy range, which confirmed the presence of MgO NPs [36]. The potassium found comes from plant compounds that remained in the extract during the preparation process [31,37]. The Mg:O weight ratios for samples (a) to (e) were determined to be 1.6, 1.56, 1.4, 1.5, and 1.3, respectively, with corresponding atomic ratios of 1.05, 1.02, 0.93, 1.00, and 0.87. Sample (d) exhibited an Mg: O atomic ratio of 1.00, which aligns most closely with the ideal stoichiometric ratio of 1:1.

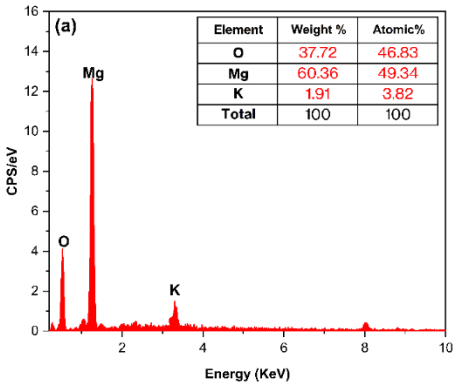

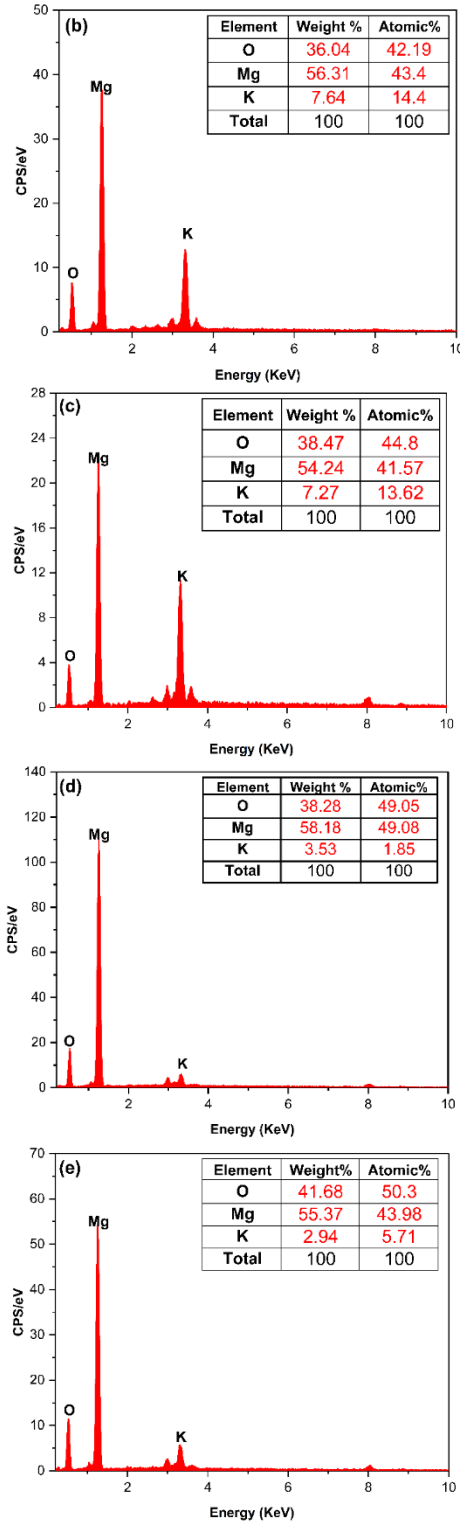

Fig. (7) EDX analysis of MgO NPs prepared in this work

The FTIR spectral of green synthesized MgO NPs showed peaks in the region 500-4000 cm^{-1} (Fig. 8). A broad peak appeared at 3412 cm^{-1}, while double peaks were observed at 2922.16 and 2850.79 cm^{-1}. Additional peaks were found at 1641.42, 1616.35, 1382.96 cm^{-1}, and in the range of 615.29–987.55 cm^{-1}. In Fig. (8), it was illustrated that FTIR peaks was at 3412 cm^{-1} (O–H stretching), 2922.16/2850.79 cm^{-1} (C–H stretching), 1641.42/1616.35 cm^{-1} (C=C stretching), and 1382.96 cm^{-1} (carbonyl stretching) underscored the involvement of plant biomolecules [38-40], while peaks at 615.29-987.55 cm^{-1} confirmed MgO formation [36,41].

The persistence of C–H (2922, 2850 cm^{-1}), C=O (1641 cm^{-1}), and O–H (3412 cm^{-1}) stretches in the MgO NPs after calcination at 500°C is unexpected, as this temperature typically combusts organic matter. We hypothesize that certain phytochemicals (e.g., polyphenols or carboxylates) form strong chemisorbed complexes with Mg^{2+} surface sites, resisting thermal decomposition. Alternatively, incomplete combustion may occur due to localized reducing environments within agglomerates. Future studies should include TGA-MS to confirm organic removal and XPS to verify surface composition. Nevertheless, the presence of Mg–O lattice vibrations (615-987 cm^{-1}) confirms successful MgO formation.

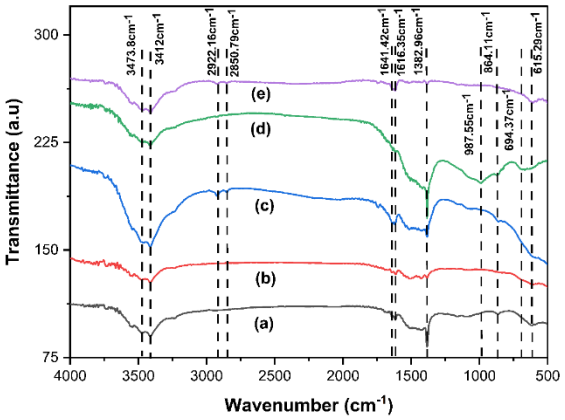

Fig. (8) FTIR spectra of MgO nanoparticles synthesized by the green method at different precursor concentrations

Five concentrations of MNH salt (table 1) were used to examine the impact of precursor concentration on biosynthesized MgO NPs using *Prunus persica* aqueous extract. UV-visible spectra of the MgO NPs were measured in the 200-800 nm range. All samples (A, B, C, D, E) exhibited strong absorption peaks at 213.8, 212, 213.8, 214, and 211.7 nm, respectively (Fig. 9). The maximum absorbance was observed at 0.3 M precursor concentration. Tauc equation was applied to obtain the energy band gap of MgO NPs [26].

$$(\alpha h\nu)^2 = A\,(h\nu - Eg)^n \qquad (2)$$

Optical properties were analyzed using diffuse reflectance spectroscopy (DRS) on dry powder samples, with $BaSO_4$ as the reference. The reflectance data (R) were converted to the Kubelka–Munk function:

$$F(R) = \frac{(1-R)^2}{2R} \qquad (3)$$

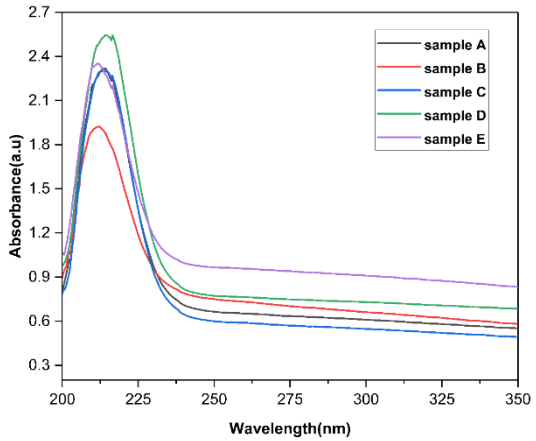

Fig. (9) UV-Visible absorption spectra of MgO NPs synthesized by the green method at different precursor concentrations

The band gap energy (E_g) was estimated from the Tauc's plot of $[F(R)\cdot h\nu]^2$ versus photon energy ($h\nu$), assuming a direct band gap transition (n = 1/2). Linear regression was applied to the rising edge of the curve (see Fig. 10), and E_g was determined by extrapolating the linear portion to the x-axis. The R^2 values of the fits ranged from 0.98 to 0.99, confirming the reliability of the band gap estimation. The band gaps for samples A–E were 5.38±0.03, 5.34±0.02, 5.38±0.03, 5.40±0.02, and 5.33±0.04 eV, respectively.

The observed band gap values (5.33-5.40 eV) are significantly lower than the bulk MgO value (~7.8 eV), which is commonly attributed to quantum confinement effects in nanoparticles. However, given the relatively large crystallite sizes (10-36nm), quantum confinement is unlikely to be the dominant factor. Instead, the reduction in band gap is likely due to defect states (e.g., oxygen vacancies, surface states) introduced during synthesis. The highest band gap (5.40 eV) at 0.3 M correlates with the most stoichiometric Mg:O ratio (1.00) and lowest agglomeration, suggesting minimized defect density rather than size reduction. This aligns with reports on defect-controlled band gap tuning in MgO NPs [21,23].

The band gap is estimated using key factors such as the absorption coefficient (α), Planck's constant (h), a material-dependent constant (A), and the energy band gap (E_g). In direct band gap, the exponent n is 1/2. To compute the band gap of MgO NPs, the plot of photon energy ($h\nu$) versus $(\alpha h\nu)^2$ was analyzed. The value was obtained by extrapolating the linear component of the curve, as seen in Fig. (10), The band gap values for samples (A to E) were found to be 5.38, 5.34, 5.38, 5.4, and 5.33 eV, respectively, which match what other researchers have found for MgO nanoparticles [21]. The highest band gap (5.40 eV) was found in sample (d) after using 0.30 M precursor concentration. Sample (e), made with the highest concentration (0.40 M), with the lowest band gap at 5.33 eV. The other samples (a), (b), and (c) had band gaps that varied slightly but stayed between 5.34 and 5.38 eV. Overall, these results show that peach leaf extract works well for making high-quality, stable MgO nanoparticles, and 0.3 M appears to be the best precursor concentration to use.

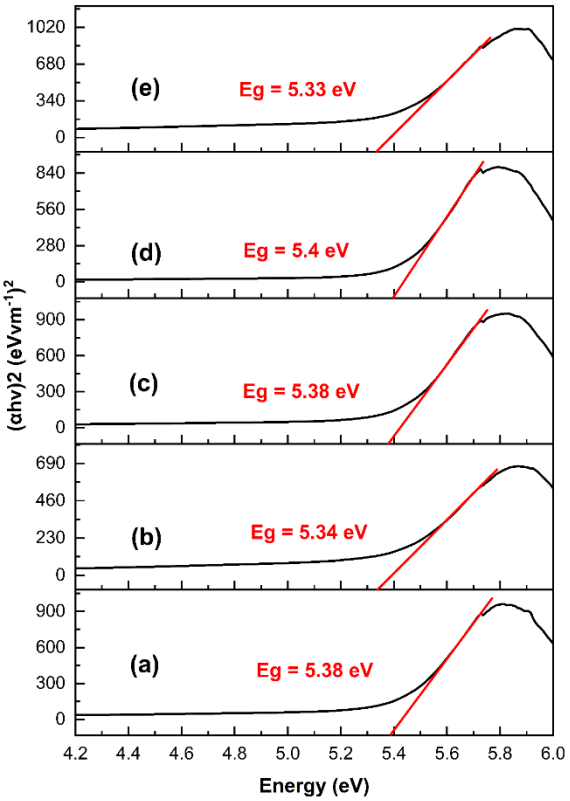

Fig. (10) Tauc plots of $(F(R).h\nu)^2$ vs. hν for MgO NPs synthesized at different concentrations. The linear region used for band gap extrapolation is marked with dashed lines

The slight reduction in band gap from 5.40 eV (0.3 M) to 5.33 eV (0.4 M) contradicts the typical quantum confinement effect (where smaller particles exhibit larger band gaps). This anomaly suggests that band structure is dominated not by size alone, but by crystallinity and defect density. The larger crystallites at 0.4 M (36.14 nm) may exhibit fewer quantum confinement effects but increased defect states (e.g., oxygen vacancies or Mg interstitials), which introduce mid-gap states and reduce the effective band gap. Conversely, the near-ideal stoichiometry (Mg:O = 1.00) and uniform morphology of the 0.3 M sample likely minimize defects, preserving a wider band gap closer to bulk MgO (7.8 eV), albeit reduced due to nanoscale effects.

4. Conclusion

This study successfully demonstrated the green synthesis of MgO nanoparticles using *Prunus persica* leaf extract. The optimal concentration yielded spherical, well-dispersed nanoparticles with near-stoichiometric composition and the widest bandgap, indicating superior structural quality. Higher or lower concentrations led to agglomeration or suboptimal

crystallinity. This precise tunability through a non-toxic, low-cost method establishes *Prunus persica* mediated synthesis as a sustainable and effective route for high-performance MgO NPs in catalytic and biomedical applications. The precise control over nanoparticle properties through simple variation of precursor concentration, coupled with the non-toxic, low-cost, and scalable nature of this green synthesis, positions *Prunus persica*-mediated MgO NPs as a promising candidate for catalytic, antibacterial, and environmental remediation applications.

References

[1] A.A. Barzinjy et al., "Biosynthesis, Characterization and Mechanism of Formation of ZnO Nanoparticles Using Petroselinum Crispum Leaf Extract", *Curr. Organ. Synth.*, 17(7) (2020) 558-566.

[2] V. Kumar, S. Munja and A. Singh, "Synthesis and Characterization of MgO Nanoparticles by Orange Fruit Waste through Green Method", *Int. J. Adv. Res. Chem. Sci.*, 4(9) (2017) 5.

[3] S. Archana et al., "Synthesis of nickel oxide grafted graphene oxide nanocomposites - A systematic research on chemisorption of heavy metal ions and its antibacterial activity", *Environ. Nanotech. Monit. Manag.*, 16 (2021) 100486.

[4] A. Ananda et al., "Green synthesis of MgO nanoparticles using Phyllanthus emblica for Evans blue degradation and antibacterial activity", *Mater. Today Proceed.*, 49 (2021) 801-810.

[5] H.R. Raveesha et al., "The electrochemical behavior, antifungal and cytotoxic activities of phytofabricated MgO nanoparticles using *Withania somnifera* leaf extract", *J. Sci.: Adv. Mater. Dev.*, 4(1) (2019) 57-65.

[6] H. Mirzaei and M. Darroudi, "Zinc oxide nanoparticles: Biological synthesis and biomedical applications", *Ceram. Int.*, 43(1) (2017) 907-914.

[7] M.A. Albrecht, C.W. Evans and C.L. Raston, "Green chemistry and the health implications of nanoparticles", *Green Chem.*, 8(5) (2006) 417-432.

[8] A. Barzinjy, A. and H. Azeez, "Green synthesis and characterization of zinc oxide nanoparticles using Eucalyptus globulus Labill. leaf extract and zinc nitrate hexahydrate salt", *SN Appl. Sci.*, 2 (2020) 3-14.

[9] Y. Ding et al., "Nanoscale magnesium hydroxide and magnesium oxide powders: Control over size, shape, and structure via hydrothermal synthesis", *Chem. Mater.*, 13(2) (2001) 435-440.

[10] K. Nagashima et al., "Epitaxial growth of MgO nanowires by pulsed laser deposition", *J. Appl. Phys.*, 101(12) (2007) 124304.

[11] J.A. Wang et al., "Characterizations of the thermal decomposition of brucite prepared by sol-gel technique for synthesis of nanocrystalline MgO", *Mater. Lett.*, 35(5-6) (1998) 317-323.

[12] L. Chen, P. Bai and W. Li, "Preparation of a novel magnesium oxide nanofilm of honeycomb-like structure and investigation of its properties", *Chem. Eng. J.*, 303 (2016) 588-595.

[13] S. Demirci et al., "Synthesis and comparison of the photocatalytic activities of flame spray pyrolysis and sol-gel derived magnesium oxide nano-scale particles", *Mater. Sci. Semicond. Process.*, 34 (2015) 154-161.

[14] H. Li et al., "Synthesis and optical properties of single-crystal MgO nanobelts", *Mater. Lett.*, 102-103 (2013) 80-82.

[15] M.A. Alavi and A. Morsali, "Syntheses and characterization of $Mg(OH)_2$ and MgO nanostructures by ultrasonic method", *Ultrason. Sonochem.*, 17(2) (2010) 441-446.

[16] A. Khan et al., "Biosynthesis and antibacterial activity of MgO-NPs produced from Camellia-sinensis leaves extract", *Mater. Res. Exp.*, 8(1) (2021) 015402.

[17] S. Abinaya et al., "Green synthesis of magnesium oxide nanoparticles and its applications: A review", *Sustain. Chem. Pharm.*, 19 (2020) 100368.

[18] M. Ramezani Farani et al., "Green Synthesis of Magnesium Oxide Nanoparticles and Nanocomposites for Photocatalytic Antimicrobial, Antibiofilm and Antifungal Applications", *Catalysts*, 13(4) (2023) 642.

[19] D.M. Roessler and W.C. Walker, "Electronic spectrum and ultraviolet optical properties of crystalline MgO", *Phys. Rev.*, 159(3) (1967) 733-738.

[20] B. Nourozi et al., "The electronic and optical properties of MgO mono-layer: Based on GGA-mBJ", *Results Phys.*, 12 (2019) 2038-2043.

[21] A.V. Jaya Srinivasan et al., "Synthesis of MgO nanoparticles for different annealing temperatures and its biomedical applications", *Nano Med. Mater.*, 3(1) (2023) 1-12.

[22] S.A. Miraeez and R.Y. Mohammed, "pH-driven green synthesis of CdO nanoparticles: H_2O_2-enhanced photocatalytic degradation of methyl orange dye in water", *Int. J. Environ. Anal. Chem.*, 106(2) (2026) 378-409.

[23] W. Arif et al., "Phytochemical Screening of Methanolic Extract of Prunus Persica", *Artic. Int. J. Sci. Res.*, 4(3) (2015) 52-53.

[24] A.U. Mirza et al., "Biogenic synthesis of iron oxide nanoparticles using *Agrewia optiva* and *Prunus persica* phyto species: Characterization, antibacterial and antioxidant activity", *J. Photochem. Photobiol. B Biol.*, 185 (2018) 262-274.

[25] R. Kumar et al., "Rapid Green Synthesis of Silver Nanoparticles (AgNPs) Using (*Prunus persica*)

Plants extract: Exploring its Antimicrobial and Catalytic Activities", *J. Nanomed. Nanotech.*, 8(4) (2017) 1000452.
[26] S.M.M. Ismail et al., "Characterization of green synthesized of ZnO nanoparticles by using pinus brutia leaves extracts", *J. Mol. Struct.*, 1280 (2023) 135063.
[27] A.U. Mirza et al., "Biogenic synthesis of iron oxide nanoparticles using Agrewia optiva and Prunus persica phyto species: Characterization, antibacterial and antioxidant activity", *J. Photochem. Photobiol. B Biol.*, 185 (2018) 262-274.
[28] R. Narayanan et al., "Theoretical study of the infrared frequencies of crystalline methyl acetate under interstellar medium conditions", *Spectrochimica Acta A : Mole. Biomole. Spectro.*, 153 (2016) 415-421.
[29] S.H. Naqvi et al., "Biological Activities and Characterization of Silver Nanoparticles from Prunus Prescia (L.) Batsch", *Lett. Appl. NanoBioSci.*, 10(3) (2021) 2466-2482.
[30] J.K. Patra and K.-H. Baek, "Green synthesis of silver chloride nanoparticles using *Prunus persica* L. outer peel extract and investigation of antibacterial, anticandidal, antioxidant potential", *Green Chem. Lett. Rev.*, 9(2) (2016) 132-142.
[31] T. Dixit, J. Suthar and S. Ravindran, "Beta vulgaris L. Extract Mediated Biogenic Synthesis of Magnesium Oxide Nanostructures and their Enhanced Antibacterial, Antioxidant, and Cytocompatibility Activities", *Polish J. Environ. Stud.*, 33(5) (2024) 4551-4559.
[32] A. Almontasser, A. Parveen and A. Azam, "Synthesis, Characterization and antibacterial activity of Magnesium Oxide (MgO) nanoparticles", *IOP Conf. Ser. Mater. Sci. Eng.*, 577(1) (2019) 012051.
[33] J. Shanmugam et al., "Green preparation of bract extract (Musa acuminate) doped magnesium oxide nanoparticles and their bioefficacy", *Appl. Organomet. Chem.*, 37(5) (2023) 1-15.
[34] M.A. Ammulu et al., "Phytoassisted synthesis of magnesium oxide nanoparticles from Pterocarpus marsupium rox.b heartwood extract and its biomedical applications", *J. Genet. Eng. Biotechnol.*, 19(1) (2021) 21.
[35] N.S.M. Saidi et al., "Synthesis and Characterization of Magnesium Oxide Nanoparticles by Using Banana Peel (*Musa acuminata Cavendish*) Extract", *Malaysian J. Anal. Sci.*, 27(5) (2023) 1017-1034.
[36] A. Muhaymin et al., "Green synthesis of magnesium oxide nanoparticles using Hyphaene thebaica extract and their photocatalytic activities", *Sci. Rep.*, 14(1) (2024) 1-12.
[37] L. Umaralikhan and M.J. Mohamed Jaffar, "Green Synthesis of MgO Nanoparticles and it Antibacterial Activity", *Iran. J. Sci. Technol. Trans. A Sci.*, 42(2) (2018) 477-485.
[38] S. Vijayakumar, M. Nilavukkarasi and P.K. Praseetha, "Synthesis of MgO nanoparticles through green method and evaluation of its antimicrobial activities", *Vegetos*, 34(3) (2021) 719-724.
[39] E.R. Essien et al., "Biogenic synthesis of magnesium oxide nanoparticles using Manihot esculenta (Crantz) leaf extract", *Int. Nano Lett.*, 10(1) (2020) 43-48.
[40] B.Y. Hirphaye et al., "Biosynthesis of magnesium oxide nanoparticles using Hagenia abyssinica female flower aqueous extract for characterization and antibacterial activity", *Appl. Water Sci.*, 13(9) (2023) 1-12.
[41] R.B. Rotti et al., "Green synthesis of MgO nanoparticles and its antibacterial properties", *Front. Chem.*, 11 (2023) 1-13.

Table (2) XRD parameters and calculated crystallite sizes for MgO nanoparticles. Instrumental broadening was corrected using a Si standard

Sample	2θ (°)	FWHM (°)	FWHM (rad)	θ (°)	Crystallite Size D (nm)	Uncertainty ± SD (nm)
A	42.81	0.65	0.0113	21.40	10.8	0.9
B	42.81	0.45	0.0078	21.40	18.1	1.2
C	42.81	0.42	0.0073	21.40	19.7	1.1
D	42.81	0.31	0.0054	21.40	27.1	1.5
E	42.81	0.23	0.0040	21.40	36.1	2.0

Table (3) Summary of average values and standard deviations from triplicate synthesis (n = 3)

Parameter	Sample A	Sample B	Sample C	Sample D	Sample E
Crystallite size (nm)	10.8 ± 0.9	18.1 ± 1.2	19.7 ± 1.1	27.1 ± 1.5	36.1 ± 2.0
SEM avg. size (nm)	125 ± 18	112 ± 15	105 ± 14	87 ± 10	130 ± 22
Band gap (eV)	5.38 ± 0.03	5.34 ± 0.02	5.38 ± 0.03	5.40 ± 0.02	5.33 ± 0.04
Mg:O atomic ratio	1.05 ± 0.02	1.02 ± 0.01	0.93 ± 0.03	1.00 ± 0.01	0.87 ± 0.02

